Spatial inhomogeneity of donor bound exciton emission from ZnO nanostructures grown on Si

M. Biswas[1], H. S. Kwack[2], D. Le Si Dang[2], M. O. Henry[1], E. McGlynn[1*]

[1] *School of Physical Sciences/National Centre for Plasma Science & Technology, Dublin City University, Glasnevin, Dublin 9, Ireland.*

[2]*Equipe CEA-CNRS-UJF Nanophysique et Semiconducteurs, Institut Néel, CNRS, Grenoble, France.*

Abstract

We report low temperature cathodoluminescence spectroscopy measurements of the band edge emission from ZnO nanostructures grown by vapour phase transport on Si. A range of donor bound exciton emission lines are found and the Al-related emission at 3.3605 eV in particular shows a marked inhomogeneity in its distribution throughout the sample. Increased 3.3605 eV emission is seen at a range of locations in nanorods and nanosheets where different nanostructures cross or coalesce, suggesting aggregation of Al donors in ZnO at regions of crystal structure disruption. However, localized crystal structure disruption appears to be a necessary rather than a sufficient condition for Al aggregation, since increased 3.3605 eV emission is seen only at such regions, but not all such regions show increased emission, implying that the microscopic nature of such regions is important in determining Al aggregation. Supporting data are presented from well-aligned, non-crossing, nanorods on *a*-sapphire.

*Author to whom correspondence should be addressed: enda.mcglynn@dcu.ie

Keywords: ZnO, nanostructure, exciton, aluminium

Introduction

ZnO is a material with large potential for UV photonics and optoelectronics. It has a large exciton binding energy (60 meV) and an excitonic bandgap at room temperature of ~ 3.3 eV, promising efficient excitonic emission at and above room temperature[1,2]. Recently, ZnO nanostructures have been the subject of intense research interest and offer great promise for device applications due to their high crystalline quality, even when grown on lattice-mismatched substrates[3]. ZnO nanostructures grown using the relatively simple method of vapour phase transport using Au catalyst layers show a diverse array of morphologies with excellent crystalline and photonic properties[3,4,5].

Doping of ZnO thin films, both n- and p-type is a heavily studied area, with important applications in transparent conducting oxides and bipolar light emitting devices[6,7]. Different dopants including N, P (p-type) and Ga, Al (n-type) are commonly used. The distribution of dopants within ZnO thin films has been studied by various authors using micro-photoluminescence (μ-PL), cathode-luminescence (CL) spectroscopy and scanning probe electrical techniques[8-10]. Evidence has been seen in many cases for inhomogeneities in the emission, and the I_0/I_1 line has been shown to be strongest at grain boundaries in heteroexpitaxial thin films, though its origin remains unclear. The peak wavelengths of the (Ga-related) I_8 line and other emissions have been shown to depend on the local strain in these samples and show greatest spectral shifts close to the substrate-film interface and also at grain boundaries where crystallites have coalesced during growth[9,10]. For homoexpitaxial thin films the dominant I_6 (Al-related) emission is reported to be quite homogeneously distributed in the sample[8].

For ZnO nanostructures to be effectively utilized in devices, it must be possible to dope these structures effectively and homogeneously. This holds both for potential uses in bipolar, p-n junction devices and in unipolar devices such as field effect transistors and field emission devices. For example, inhomogeneous doping in nanostructures used in field emission devices will lead to local hot- or cold-spots, inhomogeneous electron emission and the possibility of local burn-out of nanostructures. Although doping of ZnO nanostructures is a topic in its infancy (relatively speaking), some attempts have been reported[11,12,13,14]. Given the relatively high crystalline quality of ZnO nanostructures one might expect a homogeneous distribution of dopants within these systems (unless specific materials engineering has been undertaken, e.g. in core-shell nanostructures or embedded quantum well structures). Where data has been reported on the spatial distribution of dopant-related optical emission from ZnO nanowires acceptor dopants have been reported to be homogeneously distributed along nanowires, while evidence has suggested donors are distributed inhomogeneously[12,13].

We report low temperature cathodoluminescence (CL) spectroscopy measurements of the band edge emission from nominally undoped ZnO nanostructures grown by vapour phase transport on Si substrates. Our data show the presence of a range of donor species, deduced from the various I line donor bound exciton (DBE) emissions seen[15]. The entire range of the DBE emission shows some evidence of inhomogeneous distribution, probably partly due to variations either in CL collection efficiency or emitting volume below the incident electron beam, however the Al-related donor bound exciton emission

at 3.3605 eV ($I_{6/6a}$, 368.95 nm vacuum wavelength) displays a very marked inhomogeneity, even more so than the emission from other donor species, in its distribution throughout the sample. Increased emission intensity is seen at various locations in nanorods and nanosheets, and specifically only at certain points where different nanostructures cross or coalesce (though not at all such points), which suggests an aggregation of Al donors in ZnO at regions of either localized crystal structure disruption, consistent with a previous report and providing some clarification of the possible physical mechanism involved[12]. However, although increased $I_{6/6a}$ emission is seen only at such regions, not all such regions show increased emission, implying that the microscopic nature of the local crystal is important in determining the degree of Al aggregation.

Experimental details

The growth technique is described in more detail elsewhere[16]. Briefly, ZnO nanostructures were grown on Au-catalysed SiO_2/Si (001) substrates using the vapour phase transport (VPT) technique. The substrates were cleaned ultrasonically and a 5nm Au layer was evaporated on the substrates in a bell jar evaporator. ZnO (99.9995%) + graphite (99.9999%) powders at a 1:1 mass ratio were mixed and spread in an alumina boat. The substrates were then placed directly above the source powder on the boat with the growth surface facing the powder in a single zone tube furnace with a 90 sccm Ar carrier gas flow and with the other end of the tube open to the external atmosphere. The furnace temperature is set at 950°C and the samples were grown for 60 minutes. After growth samples were characterized by scanning electron microscopy (SEM; FEI Quanta

200) and x-ray diffraction (XRD; Bruker AXS D8 advance texture diffractometer). CL measurements were made at 5 K using a variable temperature CL setup (5-300 K) mounted on the FEI Quanta 200 SEM. The CL detection system consists of a parabolic mirror, a grating monochromator and a liquid-nitrogen-cooled CCD camera for measurements of CL spectra, and a photomultiplier tube for measurements of monochromatic CL images. CL spectra in figures 3 and 4 were obtained with similar conditions for the same sample type (i.e. on Si or sapphire substrates) but differing from one sample type to another, the sample grown on sapphire being weaker than the sample grown on Si.

Results and discussion

The 2θ-ω XRD pattern (not shown) of the deposit has been measured. All the peaks observed can be indexed either to the Si substrate or ZnO[17]. The 2θ peak values of the ZnO reflections match the reference values for unstrained ZnO to within the measurement uncertainty of ~ 0.1 ^{o} ((0002) – experiment 34.49^{o}; theory – 34.45^{o}: (10-11) – experiment 36.37^{o}; theory – 36.28^{o} : (10-12) – experiment 47.59^{o} theory – 47.58^{o}), indicating that the vast majority of the deposit is unstrained. Figure 1(a) shows a SEM image from a region of the ZnO deposit. Figures 1(b) – 1(d) show monochromatic CL-SEM images centred at 3.3661 eV (I_3 / surface exciton - SX[18]), 3.3605 eV ($I_{6/6a}$) and 3.3567 eV (I_9), respectively. The slit width used corresponds to a spread in photon energy of ~ 0.3 meV. Figure 2 shows a similar set of SEM and CL-SEM data taken from another area of the sample, with otherwise identical conditions.

The CL data from the majority of the deposit is broadly similar. In figures 1(b), 1(d), 2(b) and 2(d) there are variations in CL signal across the images. In figures 1(b) and 1(d) especially these are similar and rather gradual. These variations are related to variations in the overall CL signal levels and may indicate some inhomogeneity in distribution of both the defect species responsible for the I_3/SX and I_9 emissions. The relative heights of these peaks do not vary greatly (as shown in CL spot scans in figure 3 below) and thus the variations may also be related either to slight changes in collection efficiency in the CL system or increased volume of excited material below the probe (and in all probability are at least partly explained by such effects). However, in both figures 1(c) and 2(c) there are regions where there are clear "hot spots" of $I_{6/6a}$ emission intensity. These hot spots are labeled (i) – (iii) in figures 1 and 2. Figures 3(a) – 3(c) shows CL spot scans at the locations marked (i) – (iii) in figures 1 and 2. Figures 3(d) – 3(f) show CL spot scans at the locations marked Ref1 – Ref3 in figures 1 and 2. These data clearly show that while the intensity variations seen in figures 1(b)**,** 1(d), 2(b) and 2(d) are associated with variations in CL signal with little change in relative height of the I_3/SX and I_9 peaks, the intensity variations seen in figures 1(c) and 2(c) clearly correspond to the increased intensity (and relative intensity compared to the I_3/SX and I_9 peaks) of the specific $I_{6/6a}$ DBE line associated with the Al donor in ZnO[12]. Thus the $I_{6/6a}$ Al-related emission shows a very marked inhomogeneity, even more so than the emission from other donor species, in its distribution throughout the sample. The Al in the sample originates from contamination by the alumina boat containing the source material, which can also undergo carbothermal reduction, to a slight extent at elevated temperatures[16].

The locations (i) – (iii) in figures 1 and 2 (and all other locations of $I_{6/6a}$ emission "hot spots") correspond to locations where either we observe intersection of 2 nanostructures (e.g. (i) and (iii) in figures 1(a) and 2(a) correspond to the intersection of a nanosheet with a nanorod or a cluster) or secondary growth of one nanostructure from another (e.g. (ii) in figure 2(a)). These locations are likely, by virtue of either the coalescence or secondary growth, to be regions of either localized strain or crystal structure disruption (e.g. grain boundaries) and the data suggest that these regions act as aggregation sites for Al dopants during growth. Not all such regions (e.g. location (**) in figure 2(a)) show increased $I_{6/6a}$ emission which indicates that the microscopic nature of the local crystal is relevant in determining if Al aggregation will occur at a particular location. We note that there is no evidence that "hot spots" are associated with Au droplets, seen at certain locations (e.g. (*) in figure 1(a)).

Furthermore, while strain in ZnO nanostructures can lead to appreciable lineshifts (see e.g. Nobis *et al*[13]) in fact we see no evidence of lineshifts for the I_3/SX, $I_{6/6a}$ or I_9 lines at any of the marked locations in figures 1 and 2, as shown in figure 3. The lines occur at identical positions within the experimental uncertainty of 0.3 meV which is much less than the shifts seen by Nobis *et al*, which were of the order of some meV[13]. This is consistent with the absence of strain deduced from our XRD data. Thus we suggest that Al aggregation occurs at regions of localized crystal structure disruption such as grain boundaries and is dependent upon the microscopic nature of such structural defects.

We have tested this hypothesis by studying a ZnO nanostructure sample grown on *a*-sapphire (with very similar conditions to those described earlier and also described more fully in references 16 and 18. Nanorods grown on *a*-sapphire tend to be well-aligned normal to the substrate with no secondary growths or nanorod overlap or coalescence of the sort seen in unaligned samples grown on Si, and thus should not act as sites for Al aggregation. Cross-sectional SEM and monochromatic CL of this sample are shown in figures 4(a) – 4(d), under similar conditions to those in figure 1 and 2 (in this case figures 4(b) – 4(d) correspond to scans centered at 3.3648 eV (at the high energy side of the sample emission close to I_3/SX), 3.3601 eV ($I_{6/6a}$ / I_7) and 3.3565 eV (I_9). There is less evidence of the appearance of $I_{6/6a}$ / I_7 emission "hot spots" (and specifically no such spots are seen in the free standing nanorods which are expected to be single crystalline and do not intersect or overlap/coalesce with other nanorods or nanostructures; we note that the slightly enhanced emission at all wavelengths from location (vi) in figure 4(a) is due to two nanorods directly in line and thus both excited simultaneously by the electron beam – the enhancement is seen in all the monochromatic CL-SEM images in figures 4(b) – 4(d)). CL spot scans of the regions marked (iv) – (vii) in figure 4(a) (which show local intensity increases in figures 4(b) - 4(d)) are shown in figures 4(e) – 4(h), respectively, and reveal no very significant changes, specifically no new lines appearing from one scan to another. The intensity increases seen in figures 4(b) – 4(d) are thus mainly related to variations in the overall CL signal levels, as discussed previously. The In-related I_9 line intensity does change slightly from one scan to the next, which may indicate some degree of In aggregation in these samples (which was also seen in the samples grown on Si where some inhomogeneity in the distribution of the entire range of

the DBE emission was noted) though this does not appear related to specific morphological features identifiable in SEM. The SEM data in figure 4(a) show that the ZnO nanorods in this sample are indeed well-aligned normal to the substrate (due to mechanical effects some nanorods at the very edge of the sample have been knocked over). The growth of this sample on sapphire means that there is a stronger signal from the $I_{6/6a}$ Al-related DBE than was the case for the sample on Si, but it is seen to be quite homogeneously distributed, consistent with our hypothesis, specifically the absence of Al aggregation due to the lack of structural defects (associated with nanostructure overlap and coalescence) in the well-aligned nanorods of this sample.

Conclusions

We have measured low temperature CL data on ZnO nanostructured samples grown on both Si and sapphire. The entire range of the DBE emission shows some evidence of inhomogeneous distribution from samples grown on Si, however the effect is very much more pronounced for the Al-related $I_{6/6a}$ line and $I_{6/6a}$ "hot spots" are seen only at locations in nanorods and nanosheets where different nanostructures cross or coalesce. This is suggestive of Al aggregation at regions of localised crystal disruption in the samples such as grain boundaries, since no evidence for strain-induced lineshifts is seen. Localized crystal structure disruption appears to be a necessary rather than a sufficient condition for Al aggregation, since increased $I_{6/6a}$ emission is seen only at such regions, but not all such regions show increased emission and hence the aggregation appears to be dependent upon the microscopic nature of the structural defects. This hypothesis is consistent with further measurements of samples grown on sapphire and also with the

data of Cao *et al*, who find an inhomogeneous distribution of donors for unaligned p-doped ZnO nanostructures grown on sapphire (where Al is the dominant donor species) by pulsed laser deposition[11]. Inhomogeneous distribution of the In-related I_9 and the I_3/SX lines is also seen in the various samples but the effect is not as pronounced as for the Al-related $I_{6/6a}$ emission and specifically cannot be associated solely with locations where different nanostructures cross or coalesce. Some of the inhomgeneity in the distribution of the I_9 and the I_3/SX lines may be partly related to variations either in CL collection efficiency or emitting volume below the incident electron beam. Future studies will concentrate on elucidating the origin of this behaviour for the I_9 and the I_3/SX lines.

In conclusion, Al donors appear to be significantly affected by localised crystal structure disruption in nanostructures and display a markedly inhomogeneous distribution throughout the sample as a consequence (even more so than the emission from other donor species). The presence of structural defects leads to Al aggregation at these locations and Al-related $I_{6/6a}$ emission "hot spots". Further studies will be required to probe the microscopic details of the structural defects and correlate them with the CL emission distributions. Our findings may be important if n-doped ZnO nanostructures, doped using Al, are to be utilized for applications such as nanowire p-n junctions, field emitters etc., where dopant uniformity is a crucial parameter.

Acknowledgements

MB and EMCG acknowledge support from an SFI-RFP grant (06/RFP/PHY052).

References

1. U. Ozgur, Y. I. Alivov, C. Liu, A. Teke, M. A. Reshchikov, S. Dogan, V. Avrutin, S. J. Cho, and H. Morkoc, Journal of Applied Physics 98, art. 0413013 (2005).

2. C. Klingshirn, Physica Status Solidi (B) 244, 3027-3073 (2007).

3. Z. L. Wang, Materials Today 7, 26-33 (2004).

4. P. D. Yang, H. Yan, S. Mao, R. Russo, J. Johnson, R. Saykally, N. Morris, J. Pham, R. He, and H.-J. Choi, Advanced Functional Materials 12, 323-331 (2002).

5. R.T. Rajendra Kumar, E. McGlynn, C. McLoughlin, S. Chakrabarti, R. C. Smith, J. D. Carey, J.P. Mosnier , and M.O. Henry, Nanotechnology 18, art. 215704 (2007).

6. K. Ellmer, J. Phys. D: Appl. Phys. 34, 3097-3108 (2001).

7. A. Tsukazaki, A. Ohtomo, T. Onuma, M. Ohtani, T. Makino, M. Sumiya, K. Ohtani, S. F. Chichibu, S. Fuke, Y. Segawa, H. Ohno, H. Koinuma, and M. Kawasaki, Nature Materials 4, 42-46 (2005).

8. H. von Wenckstern, H. Schmidt, C. Hanisch, M. Brandt, C. Czekalla, G. Benndorf, G. Biehne, A. Rahm, H. Hochmuth, M. Lorenz, and M. Grundmann, Physica Status Solidi (RRL) 1, 129-131 (2007).

9. F. Bertram, D. Forster, J. Christen, N. Oleynik, A. Dadgar, and A. Krost, Journal of Crystal Growth 272, 785-788 (2004).

10. F. Bertram, D. Forster, J. Christen, N. Oleynik, A. Dadgar, and A. Krost, Applied Physics Letters 85, 1976-1978 (2004).

11. M. Yan, H. T. Zhang, E. J. Widjaja, and R. P. H. Chang, Journal of Applied Physics 94, 5240-5246 (2003).

12. B. Q. Cao, M. Lorenz, A. Rahm, H. Von Wenckstern, C. Czekella, J. Lenzner, G. Benndorf, and M. Grundmann, Nanotechnology 18, art. 455707 (2007).

13. T. Nobis, E.M. Kaidashev, A. Rahm, M. Lorenz, J. Lenzner, and M. Grundmann, Nano Letters 4, 797-800 (2009).

14. H.J. Zhou, J. Fallert, J. Sartor, R.J.B. Dietz, C. Klingshirn, H. Kalt, D. Weissenberger, D. Gerthsen, H.B. Zeng, and W.P. Cai, Applied Physics Letters 92, art. 132112 (2008).

15. B. K. Meyer, H. Alves, D. M. Hofmann, W. Kriegseis, D. Forster, F. Bertram, J. Christen, A. Hoffmann, M. Strabburg, M. Dworzak, U. Haboeck, and A. V. Rodina, Physica Status Solidi (b) 241, 231-260 (2004).

16. J.-R. Duclère, B. Doggett, M. O. Henry, E. McGlynn, R. T. Rajendra Kumar, J.-P. Mosnier, A. Perrin, and M. Guilloux-Viry, Journal of Applied Physics 101, art. 013509 (2007).

17. ZnO: JCPDS Card No. 36-1451; Si: JCPDS Card No. 27-1402.

18. J. Grabowska, A. Meaney, K.K. Nanda, J.-P. Mosnier, M.O. Henry, J.R. Duclère, and E. McGlynn, Phys. Rev. B 71, art.115439 (2005).

Figure Captions

Fig. 1. (a) SEM image from a region of the ZnO deposit; Monochromatic CL images centred at (b) 3.3661 eV (I_3/SX), (c) 3.3605 eV ($I_{6/6a}$) and (d) 3.3567 eV (I_9). Region (*) in figure 1(a) shows a Au droplet atop a nanorod.

Fig. 2. (a) SEM image from a different region of the ZnO deposit; Monochromatic CL-SEM images centred at (b) 3.3661 eV (I_3/SX), (c) 3.3605 eV ($I_{6/6a}$) and (d) 3.3567 eV (I_9).

Fig. 3. (a) – (c) CL spot scans at the locations marked (i) – (iii) in figures 1 and 2; (d) – (f) CL spot scans at the locations marked Ref1 – Ref3 in figures 1 and 2, respectively.

Fig. 4. (a) SEM of sample grown on *a*-sapphire; Monochromatic CL images centred at (b) 3.3648 eV (at the high energy side of the sample emission), (c) 3.3601 eV ($I_{6/6a}$ / I_7) and (d) 3.3565 eV (I_9); (e) – (h) CL spot scans from regions (iv) – (vii) marked in figure 4(a), respectively.

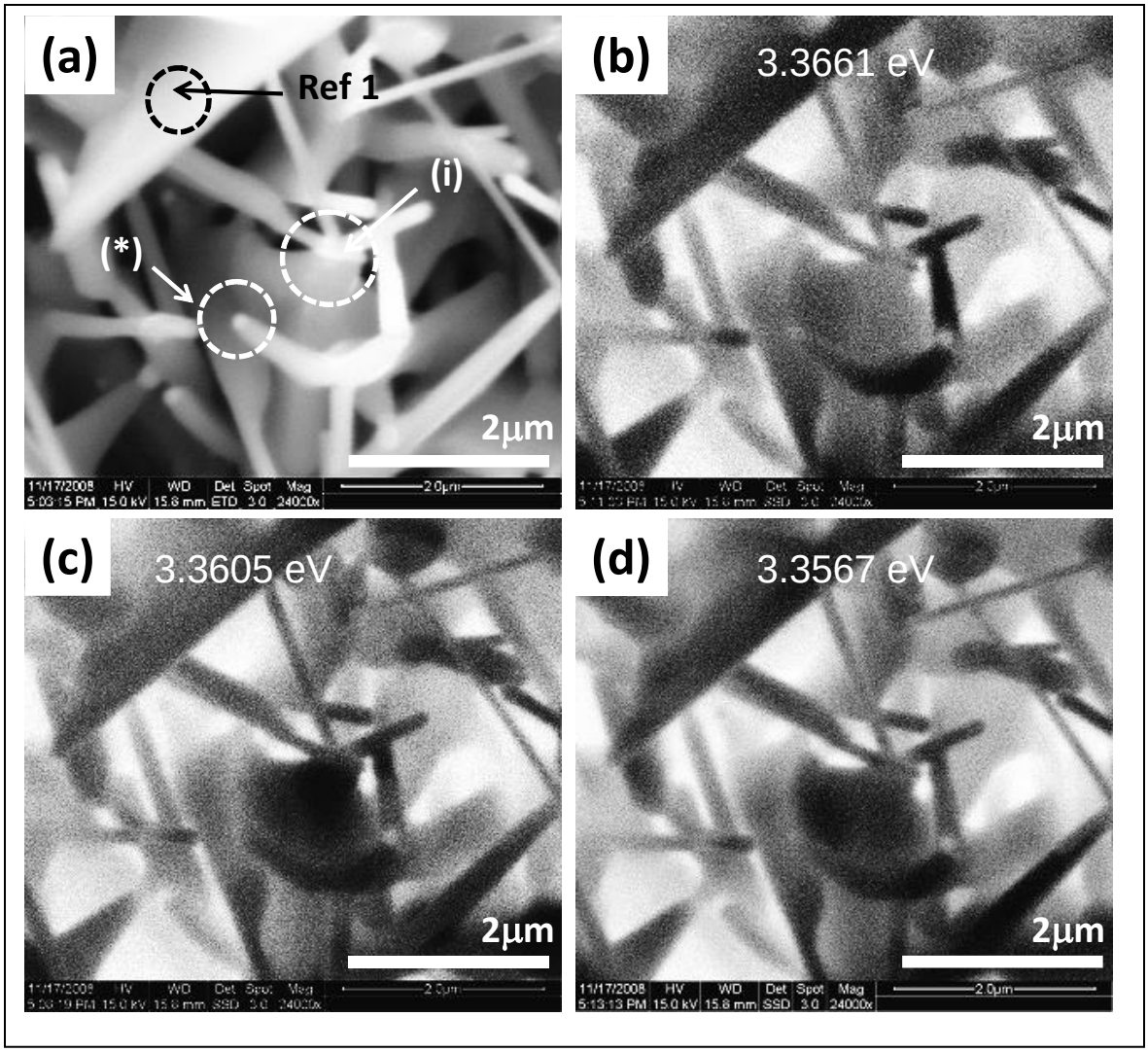

Figure 1: Biswas *et al*

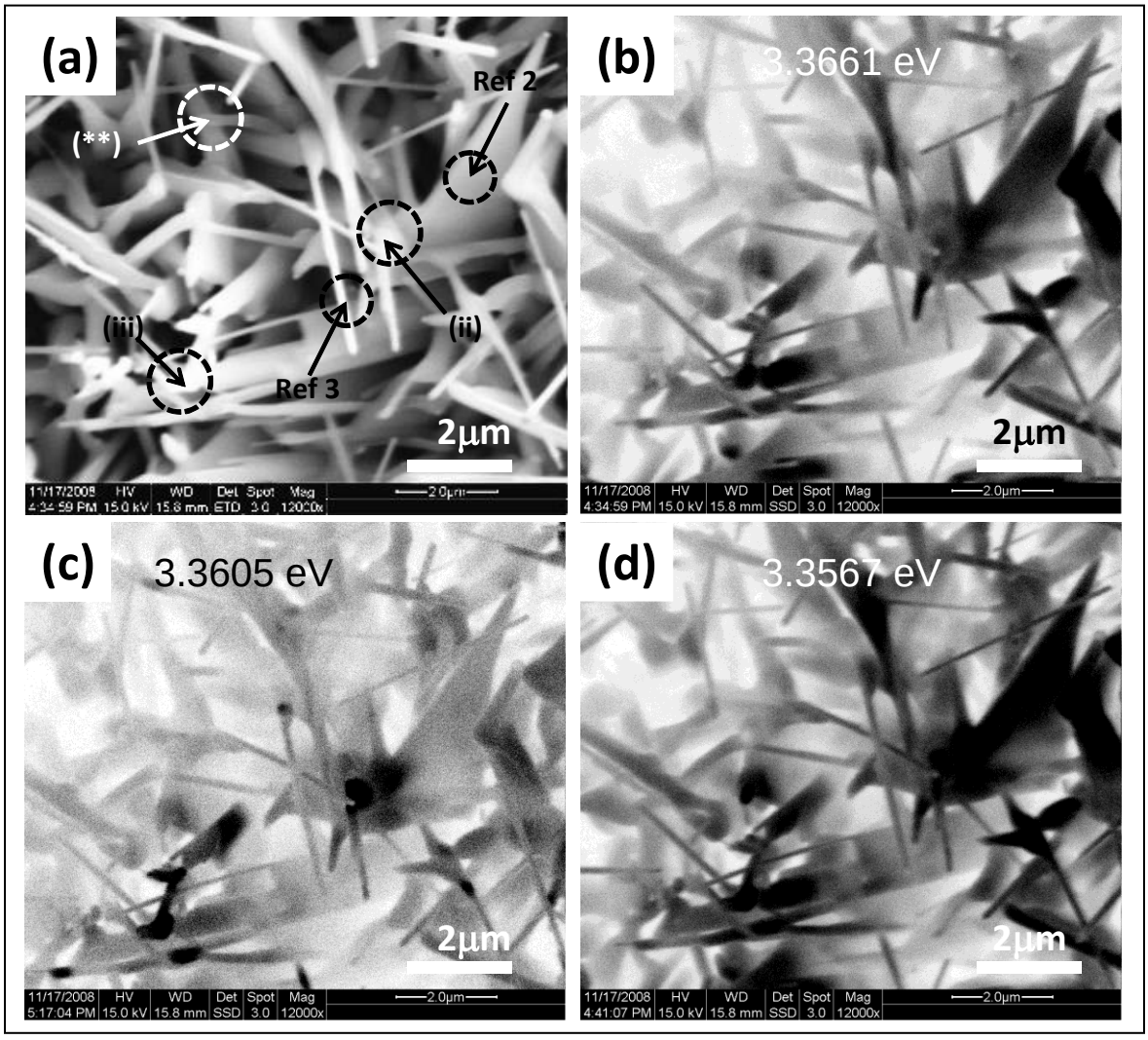

Figure 2: Biswas *et al*

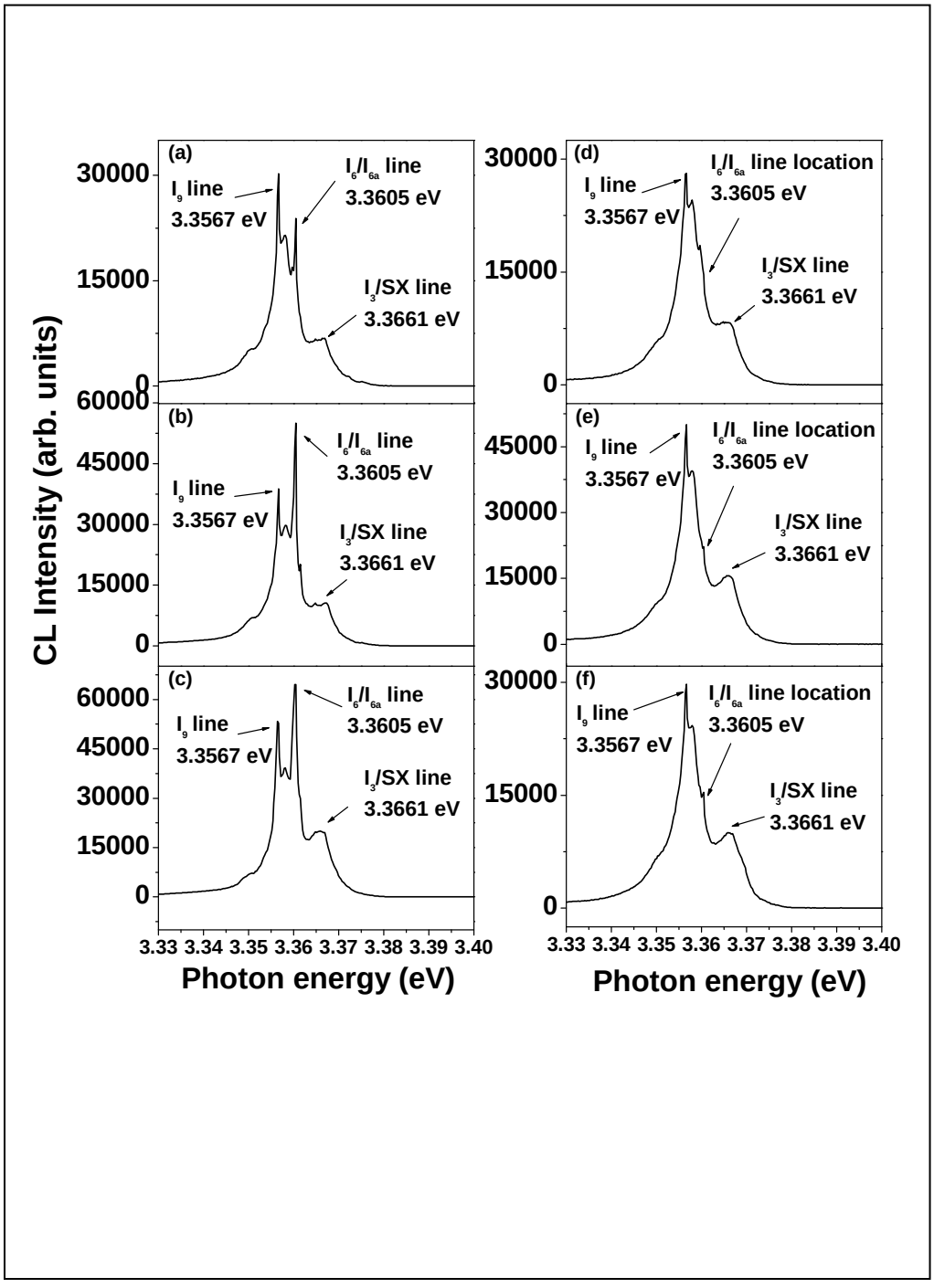

Figure 3: Biswas *et al*

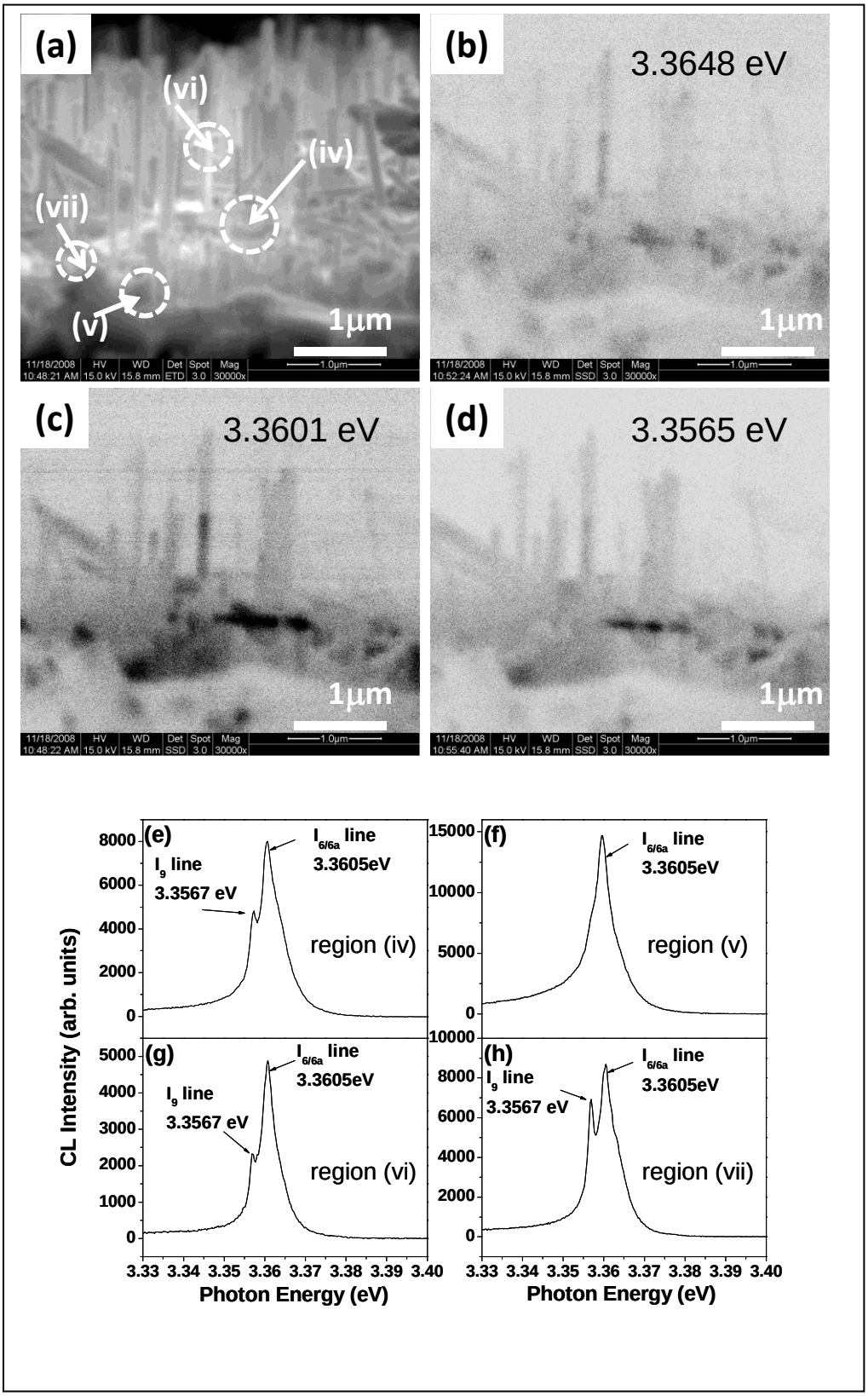

Figure 4: Biswas *et al*